

Live Cell Lineage Tracing of Dormant Cancer Cells

Hyuna Kim, Anna Wirasaputra, Farnaz Mohammadi, Aritra Nath Kundu, Jennifer A. E. Esteves, Laura M. Heiser, Aaron S. Meyer, and Shelly R. Peyton*

Breast cancer is a leading cause of global cancer-related deaths, and metastasis is the overwhelming culprit of poor patient prognosis. The most nefarious aspect of metastasis is dormancy, a prolonged period between primary tumor resection and relapse. Current therapies are insufficient at killing dormant cells; thus, they can remain quiescent in the body for decades until eventually undergoing a phenotypic switch, resulting in metastases that are more adaptable and drug resistant. Unfortunately, dormancy has few in vitro models, largely because lab-derived cell lines are highly proliferative. Existing models address tumor dormancy, not cellular dormancy, because tracking individual cells is technically challenging. To combat this problem, a live cell lineage approach to find and track individual dormant cells, distinguishing them from proliferative and dying cells over multiple days, is adapted. This approach is applied across a range of different in vitro microenvironments. This approach reveals that the proportion of cells that exhibit long-term quiescence is regulated by both cell intrinsic and extrinsic factors, with the most dormant cells found in 3D collagen gels. This paper envisions that this approach will prove useful to biologists and bioengineers in the dormancy community to identify, quantify, and study dormant tumor cells.

H. Kim, S. R. Peyton
 Molecular and Cell Biology Graduate Program
 University of Massachusetts
 Amherst, MA 01002, USA
 E-mail: speyton@ecs.umass.edu

A. Wirasaputra, A. N. Kundu, S. R. Peyton
 Department of Chemical Engineering
 University of Massachusetts
 Amherst, MA 01002, USA

F. Mohammadi, A. S. Meyer
 Department of Bioengineering
 University of California
 Los Angeles, CA 90095, USA

J. A. E. Esteves, S. R. Peyton
 Department of Biomedical Engineering
 University of Massachusetts
 Amherst, MA 01002, USA

L. M. Heiser
 Department of Biomedical Engineering
 Knight Cancer Institute
 Oregon Health & Science University
 Portland, OR 97239, USA

A. S. Meyer
 Jonsson Comprehensive Cancer Center
 University of California
 Los Angeles, CA 90095, USA

 The ORCID identification number(s) for the author(s) of this article can be found under <https://doi.org/10.1002/adhm.202202275>

DOI: 10.1002/adhm.202202275

1. Introduction

2.3 million women worldwide were diagnosed with breast cancer in 2020, with approximately 685 000 reported deaths.^[1,2] The five-year survival rate varies based on region and breast cancer subtype, with 85%–90% survival in high-income countries and 60% or lower in many developing countries.^[3,4] It is important to note, however, that these statistics are associated with reporting disparities from lower-middle income areas.^[5]

When breast cancer is stage I or II, tumor growth can be controllable with chemotherapy, surgery, and radiation, and the five-year survival rate is 90%–100% in the United States.^[6,7] However, when breast cancer metastasizes to other organs, the survival rate dramatically decreases to 22%.^[8] Breast cancer commonly metastasizes to bone, lung, brain, and liver. Even after initially successful treatment, 13%–30% of early-stage breast cancer patients develop cancer relapse in distant organs, most frequently

in the bone.^[9,10] This indicates that disseminated tumor cells (DTCs) can remain dormant for many years, even decades, before growing into a detectable, symptomatic tumor.^[9,10] It is difficult to treat these dormant cells as traditional chemotherapies target rapidly growing cells. Also, regardless of their cell cycle status, DTCs are actively protected by their microenvironment and vascular endothelium.^[11]

Dormancy is categorized either as tumor mass dormancy or cellular dormancy. Tumor mass dormancy states that the rate of cancer cell proliferation in a bulk of tumor equals that of cell death.^[12] Cellular dormancy is instead a result of an individual DTC temporarily exiting the cell cycle and remaining in a quiescent state, with the possibility that it can resume proliferation later.^[12] Researchers have been studying the critical factors and the molecular mechanisms governing dormancy and subsequent relapse, but it is challenging to find and track individual DTCs that are both viable and dormant. For instance, immunohistochemistry (IHC) of fixed clinical and *in vivo* specimens can provide insight into localization of dormant or proliferating cells within the matrix by comparing the levels of Ki-67 expression.^[13,14] However, IHC cannot determine if the observed nonproliferative cells are capable of eventual outgrowth, nor if the factors from their microenvironment would affect the outgrowth because the process is limited to fixed samples.

Moreover, most traditional *in vitro* models fail to capture the interactions between cancer cells and their microenvironment.

Currently, the majority of dormancy models exist as 2D systems, mainly plastic or protein-treated coverslips, due to ease of use and greater reproducibility. While it yields more consistent results, the differences between these 2D systems and native tissue present many limitations. One of the biggest differences involves tumor cell morphology and how a flat versus spherical geometry changes the adhesion of the cells to the extracellular matrix (ECM) and the drug efficacy of certain treatments. Thus, there is a greater push to develop novel 3D environments using either polyethylene glycol (PEG) or polyacrylamide, though less than 20% of papers reviewed from Micalet et al. contained these systems.^[1] These 3D models are favored over the 2D systems as they mimic more accurate cell behavior in the body by providing similar mechanical and chemical properties of the body's premetastatic niches. For instance, a bioinspired 3D growing environment for predominantly ER+ cancer cells (T47D and BT474) more accurately identified key differences in ECM compositions for late relapse events.^[16] Similarly, the Slater lab developed tunable RGD hydrogels that allowed in-depth studies of dormancy reactivation by changing the chemical and mechanical properties and identifying phenotypic switches for encapsulated MDA-MB-231 cells.^[17] Another example of showing the interactions between cancer cells and their microenvironment, derived via intravital imaging, showed that certain microenvironments, like perivascular niches, protect DTCs from chemotherapy.^[11] The overwhelming advantage of intravital imaging is the ability to watch DTCs in an *in vivo* context, but is expensive, difficult to learn, and low throughput. We see intravital imaging as an excellent way to test specific hypotheses, but not well-suited for screening larger numbers of conditions. Creating *in vitro* approaches to observe cell quiescence and reactivation are sorely needed to better understand the factors that lead to relapse, such as that demonstrated here.

In order to track cell plasticity with greater accuracy, the Heiser lab developed a method to classify cells according to their heterogeneous phenotypes across lineages.^[18] We adapted this model to create cell lineage trees and analyze individual cell proliferation and death. This method solves several problems with other commonly used cell proliferation assays. For example, the MTT assay is an endpoint assay, and it often overestimates cell viability.^[19] Immunofluorescent (IF) staining, a commonly used method for assessing protein expressions, is also an endpoint assay which requires cell fixation. Live microscopy and manual tracking of cells through this lineage tracking allowed us to find and distinguish quiescent cells from proliferating and dying cells. We present this approach here, validated with established markers of cellular dormancy, to demonstrate the emergence of dormant populations across a variety of cell culture environments.

2. Results

2.1. IHC Subtypes of Breast Cancer Cell Lines Correlate with Observed Proliferation and Dormancy Rates

HCC1954 is a HER2 enriched (HER2+) ER- breast cancer cell line, which is a subtype correlated with more metastasis in the clinic, and more proliferative than luminal A type cell lines such as MCF7 (from Cellosaurus). We observed the HCC1954 cell lineage trees to have a higher distribution of cells prolifera-

ting twice or more than those in MCF7 (Figure 1a,b and Figure S1a,b, Supporting Information), as expected. More than 50% of the randomly selected HCC1954 cells divided twice or more (Figure 1a,b). According to Cellosaurus, a cell ancestry database, HCC1954 has a doubling time of 45 h and MCF7 has a maximum doubling time of 80 h, which further validates the difference in cell proliferation between the two cell lines. When comparing the cell lineage trees of HCC1954 and MCF7 cultured on tissue culture polystyrene (TCPS), there are a smaller number of nondividing cells, illustrated as a single straight line across the graph, in HCC1954 than in MCF7 (Figure 1a,b and Figure S1a,b, Supporting Information). In this paper, we define the nondividing live cells as "dormant" cells, as they do not divide and do not die but rather persist over the entire course of the experiment.

2.2. Dormant Cell Population Increases on Glass Coverslips Compared to That on TCPS

We tracked cells on glass substrates that were chemically functionalized with individual cell proteins or peptides, as we have described elsewhere.^[20,21] Collagen and collagen-derived peptides (GFOGER) were chosen based on our prior work that demonstrated collagen I-functionalized surfaces as supporting cell entrance into dormancy *in vitro*.^[22] Cell attachment was overall lower on these protein- and peptide-functionalized glass coverslips, and we also observed higher rates of cell death than those on TCPS (Figure 1a,b,e-h). To ensure equal numbers of cells attached to the surfaces, we seeded cells at a higher density on protein- and peptide-functionalized surfaces. The number of dormant cells was higher on glass coverslips than on TCPS (*p*-value = 0.36, *n* = 3). Overall, the dormant cell population on both the rat tail collagen I-functionalized and the collagen I peptide (GFOGER)-functionalized coverslips had similar trends (Figure 1f-h, Supporting Information); however, the cells seeded on the GFOGER-functionalized coverslips had a lower number of cells that divided twice or more than the cells seeded on the collagen I protein-functionalized coverslips (Figure 1h). In addition, cells cultured on the protein- or peptide-functionalized coverslips had a higher portion of dormant cells while had lower cell death than the control, phosphate buffered saline (PBS)-treated coverslips (Figure 1e-h). Specifically, collagen I drove higher numbers of dormant cells compared to the PBS and GFOGER-treated coverslips (*p*-values of 0.044 and 0.19, respectively). Together, this tells us that collagen-functionalized glass coverslips allow cells to undergo dormancy, and the form of collagen—either whole collagen protein or a part of the protein which is GFOGER peptide—does not have a significant effect on dormant cell population.

2.3. Higher Proportions of Dormant Cells Are Found in 3D Environments

Matrigel and collagen gels are commonly used materials for cancer studies as collagen is the most abundant protein in human connective tissues, and Matrigel is ECM extracted from Engelbreth-Holm-Swarm mouse tumors.^[23] When MCF7 and HCC1954 cell lines were cultured on 2D Matrigel, both were less proliferative in comparison to TCPS (Figures 1b and 2b;

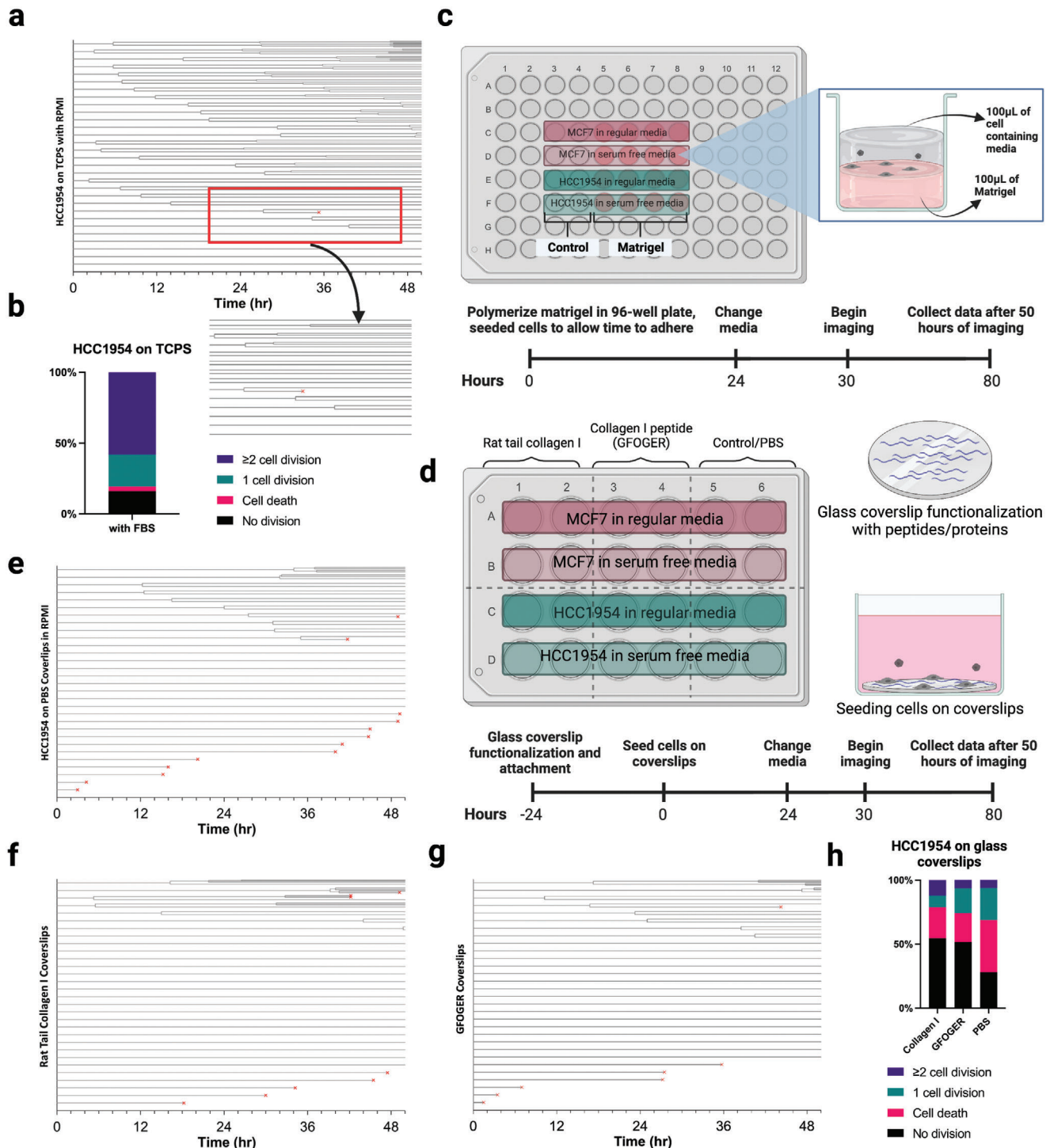


Figure 1. Experimental setups and timelines for 2D environments. a) A cell lineage tree of HCC1954 cells on TCPS obtained by randomly tracking 30 individual cell proliferation across 50 h. Each time a cell splits, it is denoted in the graph by splitting into two lines. Increasing on the y-axis shows least proliferating to most. If a cell does not split, it will have a straight line across the entire graph. When encountering a dying cell, the time of death is marked with a red "x". b) Bar graph distribution of cell division and death from the lineage analysis. c) This schematic consists of the seeding procedure and experimental timeline of two cell lines (MCF7 and HCC1954) in different media conditions on top of 2D Matrigel in a 96-well plate. d) Schematic of a 24-well plate containing protein-treated coverslip conditions with an included timeline. Cell lineage analyses of HCC1954 in serum containing media (RPMI) across the coverslip conditions: e) PBS-treated coverslip, f) Collagen I protein-treated coverslip, and g) Collagen I peptide (GFOGER)-treated coverslip. h) Stacked bar graph for coverslip conditions from (e)–(g).

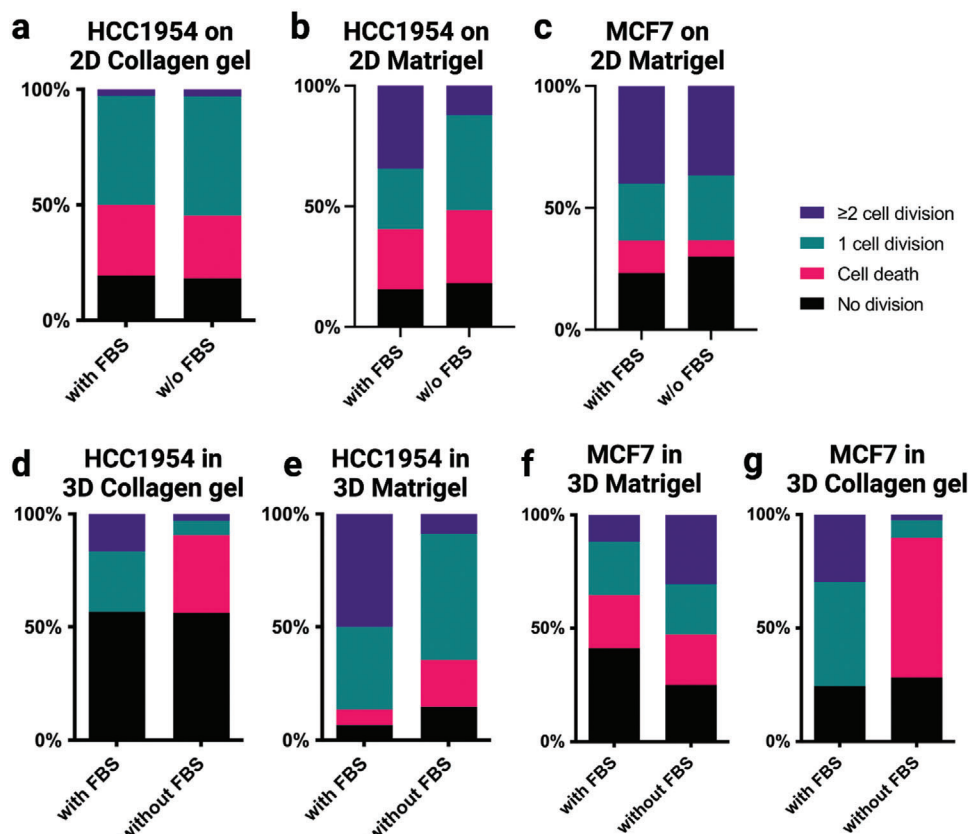


Figure 2. Distribution of cell proliferation in 2D and 3D gel environments. a) The stacked bar graph showing proportion of cells with 0, 1, 2+ cell divisions or with cell death, which data were taken from the cell lineage analysis conducted on HCC1954 cells seeded on 2D collagen gel in regular RPMI. Bar graphs showing proportion of cells with 0, 1, 2+ cell divisions or with cell death for b) HCC1954 and c) MCF7 cells on 2D Matrigel. d) Bar graphs showing proportion of cells with 0, 1, 2+ cell divisions or with cell death for HCC1954 in 3D collagen gel. e) Bar graphs showing proportion of cells with 0, 1, 2+ cell divisions or with cell death for MCF7 in 3D Matrigel. f) Stacked bar graphs showing proportion of cell populations with 0, 1, 2+ cell divisions or with cell death for MCF7 in 3D collagen gel.

Figures S1 and S2, Supporting Information). The HCC1954 line also had a greater number of deaths over the course of the experiment for both serum-containing and serum-free media conditions (Figure 2b). This suggests those cells have a greater sensitivity to serum deprivation, which we also observed in a previous dormancy study.^[22] In addition, both cell lines cultured on 2D Matrigel appeared to have lower proliferation than when cultured on TCPS, which could be due to the relative softness of Matrigel, which is known to influence cell proliferation rates.^[24,25] However, the dormant cell population does not significantly change in both cell lines on 2D Matrigel compared to those on TCPS (Figures 1a,b and 2b,c; Figures S1 and S2a,b, Supporting Information). MCF7 cells showed less cell death on 2D Matrigel (Figure 2c and Figure S2a, Supporting Information) while HCC1954 suffered more cell death (Figure 2b and Figure S2b, Supporting Information). Also, there were more dormant MCF7 cells observed after 50 h in culture (Figure 2c and Figure S2a, Supporting Information) than HCC1954 (Figure 2b and Figure S2b, Supporting Information), in both serum-containing and serum-free growth media conditions. Taken together, the 2D Matrigel environment does not have a significant effect on dormant cell populations in both HCC1954 and MCF7, but the dormant cell

population differs by cell line, which means the IHC subtypes of breast cancer cell lines play more significant role in dormancy than the 2D Matrigel environment itself does.

Significant differences in cell growth behavior, especially the dormant cell population, were observed when compared these cell lines on the same ECM protein in 2D versus 3D (*p*-value 0.002). HCC1954 cells were cultured on 2D collagen gels and in 3D collagen gels; more than 50% cells were dormant in 3D collagen gel environment (Figure 2d and Figure S3b, Supporting Information) while fewer than a quarter of the cells were dormant when cultured on a 2D collagen gel (Figure 2a and Figure S2c, Supporting Information). Interestingly, about the same number of cells were dormant for 50 h in both serum-containing and serum-free conditions in 3D collagen gels, but there were greater numbers of cells dying in the 3D collagen material than 2D (Figure 2d and Figure S3b, Supporting Information). While the 3D collagen environment resulted in a higher number of dormant cells than 2D collagen gel environment, it showed the opposite trend in Matrigel. There were a greater number of dormant cells on 2D Matrigel (Figure 2b and Figure S2b, Supporting Information) than in 3D Matrigel (Figure 2e and Figure S3a, Supporting Information). In addition, when comparing the matrix materials

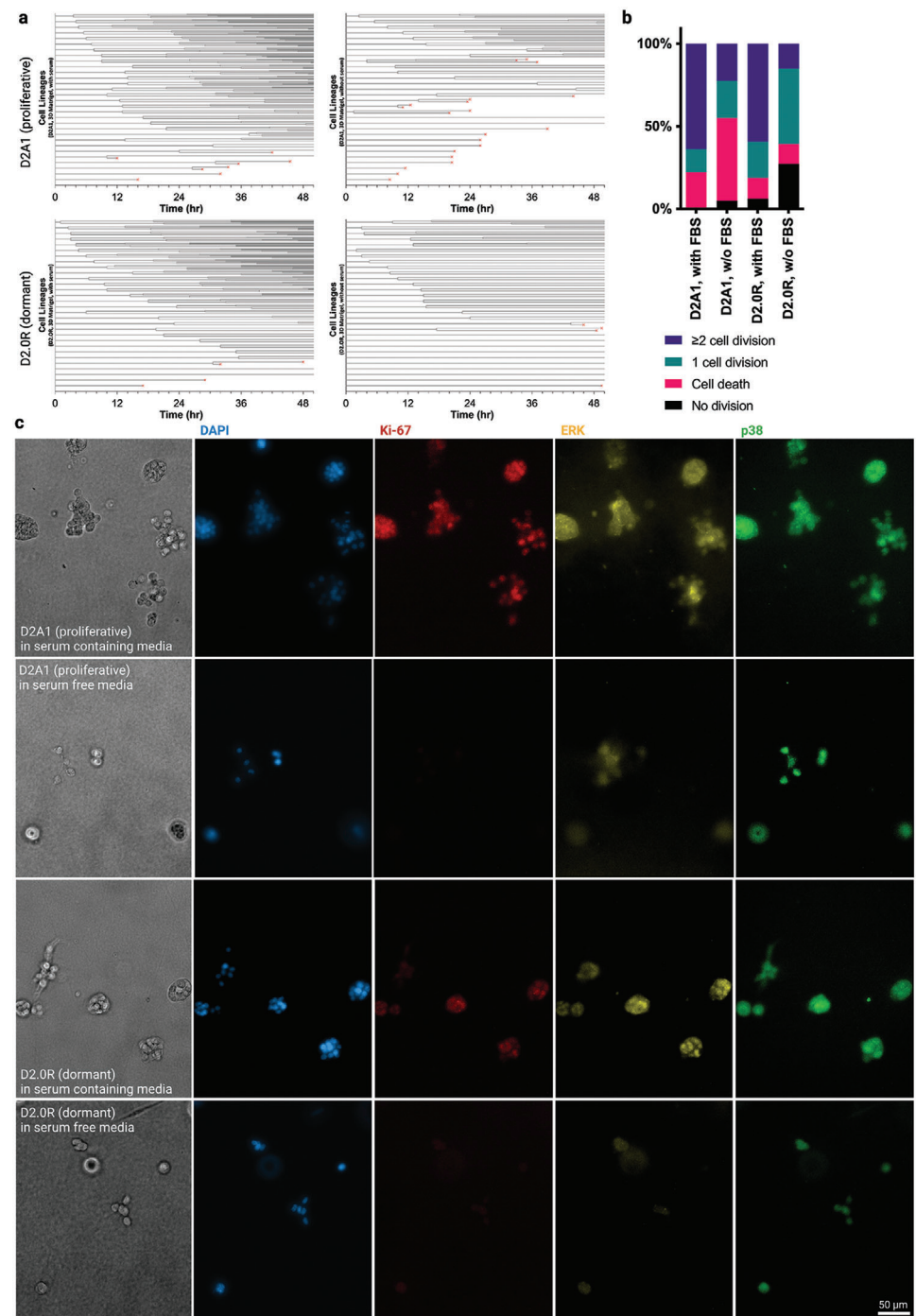


Figure 3. Mouse breast cancer cells that have a proliferative (D2A1) or dormant (D2.0R) phenotype in 3D Matrigel. a) Cell lineage trees of D2A1 (proliferative) and D2.0R (dormant) cells in serum-containing and serum-free conditions. Top row is showing D2A1 lineages, and bottom row is showing D2.0R lineages. Left column is the lineage trees of cells under the serum-containing condition, and right column is the lineage trees of cells under serum-free condition. b) A stacked bar graph showing the proportion of cells with 0, 1, 2+ cell divisions or with cell death of D2 series cells. The number of each group was calculated from the cell lineage trees shown in (a). c) IF staining images of D2 series cells in serum-containing and serum-free conditions. Images on the far-left column are brightfield images, and the images from second to fifth columns are IF staining images. Cells were stained with DAPI (blue), Ki-67 (red), ERK (yellow), and p38 (green). Scale bar = 50 μ m. d) Quantification of fluorescent levels of Ki-67, ERK, and p38 in each condition. Scattered plot of ERK and p38 expression levels in individual cells of e) D2A1 and f) D2.0R. Each dot indicates data from a single cell.

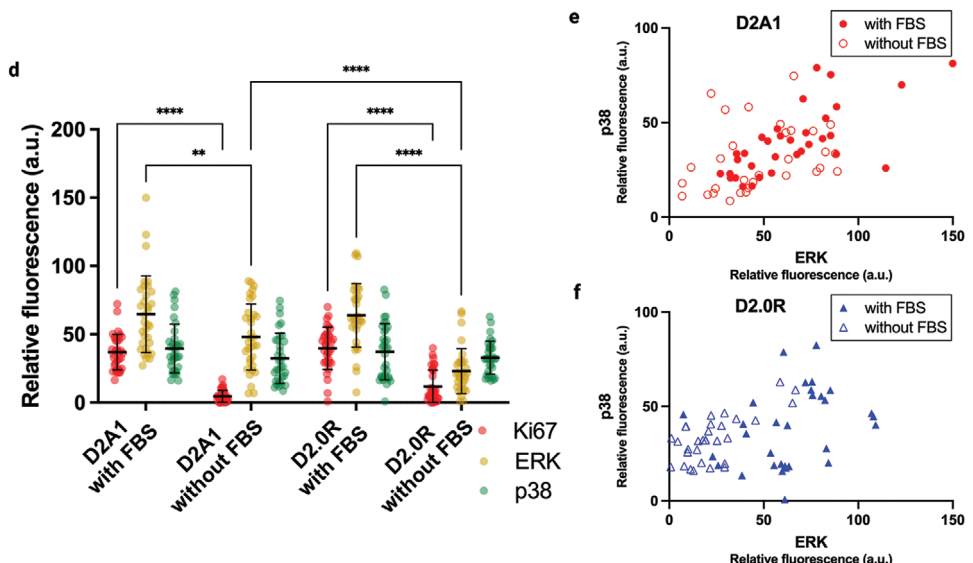


Figure 3. Continued

in the same dimension, 2D collagen gel versus 2D Matrigel, for example, the matrix material does not play a significant role in dormancy when it is on 2D (Figure 2a,b); however, when it is in 3D, there was a significant difference in dormant cell population between cells in 3D collagen gels and those in 3D Matrigel. These results show that the types of matrix materials have a greater effect in 3D than on 2D. In HCC1954 cells, we observed higher proportions of dormant cells in 3D collagen compared to 3D Matrigel (*p*-value 0.0001 with FBS, *p*-value 0.0006 without FBS), and MCF7 cells had an insignificant similar trend (*p*-value 0.2 with FBS, *p*-value 0.8 without FBS) (Figure 2f,g and Figure S3c,d, Supporting Information).

2.4. Immunofluorescence Staining Validates the Cell Lineage Tree Approach to Identify Dormant Cells

Two different mouse breast cancer cell lines from the same origin were used to validate if the cell lineage tree analysis is a viable method to use for dormancy study. D2A1 is a proliferative cell line and D2.0R is a dormant cell line.^[26–29] Both cell lines showed high proliferation in serum-containing medium in 3D Matrigel (Figure 3a,b). A significant difference in dormancy (*p*-value 0.018) between these two cell lines was observed when they were cultured in serum-free media. D2.0R, the dormant cells, showed less cell death and more dormant phenotypes in serum-free environment than D2A1, the proliferative cells, and there were more nondividing alive D2.0R cells when cultured in serum-free media than in serum-containing media (Figure 3a,b). This result supports an earlier study that showed that serum deprivation forced cells into dormant-like state.^[22]

Cells were immunofluorescently stained with Ki-67, ERK, p38, and DAPI to validate that the differences we saw in numbers of dormant cells using cell lineage tracking was reflected by the standard set of markers used to identify dormant cells. Dormant cells are distinguished by low Ki-67, low ERK, and high p38 expression.^[30,31] Both Ki-67 and ERK expression were sig-

nificantly lower in each cell line without FBS than with FBS, but there was no significant difference observed when comparing between D2A1 and D2.0R in serum-containing media (Figure 3c,d). There were relatively few dormant cells (ERK-low and p38-high) in serum-containing environments for both cell lines (Figure 3c,e,f). D2.0R cells showed significantly lower ERK expression than the D2A1 cells when cultured in serum-free conditions (Figure 3c,d). The D2.0R cells cultured in 3D Matrigel without serum had the most cells that were positive for dormancy markers (low ERK and high p38) than any other conditions (Figure 3c–f), validating our results from the cell lineage tree analyses.

2.5. TNBC Cells Did Not Show Significant Differences in Dormant Cell Populations with or without Serum in 3D Environments

Breast cancer recurrence rates and regions vary depending on its molecular subtype. For example, triple negative breast cancer (TNBC) accounts for 10–20% of all breast cancer cases, but it is highly aggressive and heterogeneous, and it has the highest recurrence rate in the first five years.^[16,32] Although this is not a subtype that typically results in clinical dormancy, we wanted to see if this approach could in fact capture small numbers of cells that could be forced into a nonproliferative state and monitored. We performed experiments with two different human TNBC cell lines: MDA-MB-231 and HCC1143. We cultured them in 3D collagen gels and Matrigel with or without serum. Unlike MDA-MB-231s on TCPS, which showed significant differences in non-dividing cell populations (*p*-value < 0.0005), neither HCC1143 nor MDA-MB-231 cells were significantly different in the number of nondividing cells in 3D collagen or Matrigel (Figure 4a–c and Figure S4a–c, Supporting Information). Regarding MDA-MB-231 cells, although the numbers of dormant cells were higher in serum-free condition than in serum-containing condition in 3D collagen (*p*-value 0.42) and Matrigel (*p*-value 0.16), they were

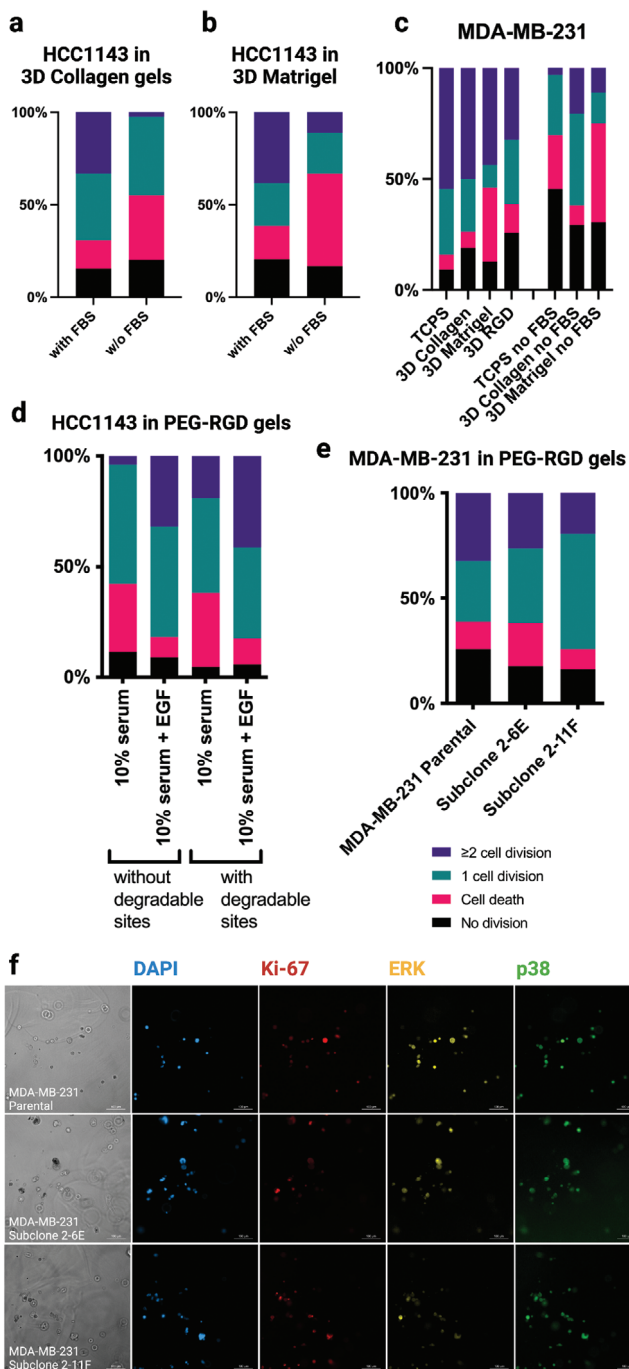


Figure 4. Triple negative breast cancer lines in PEG-RGD gels. Stacked bar graphs from the cell lineage analysis conducted on HCC1143 cells in a) 3D collagen and b) 3D Matrigel. c) Stacked bar graphs from cell lineage analysis of MDA-MB-231 cells on TCPS and in various 3D environments. Four columns on the left are with FBS, and three columns on the right are without FBS. d) A stacked bar graph from the cell lineage analysis conducted on HCC1143 cells in a 3D PEG-RGD system with different serum and EGF conditions. e) Bar graph of the MDA-MB-231 cell line with its subclones 2-6E and 2-11F in 3D PEG-RGD gels. f) IF-stained images of MDA-MB-231 parental and subclones in 3D PEG-RGD gels with FBS. DAPI is shown in blue, Ki-67 in red, ERK in yellow, p38 in green. Scale bar = 100 µm.

not statistically significant (Figure 4c). We also did not observe a difference when comparing between the 3D materials (p -value 0.76 for 3D collagen vs Matrigel with FBS, and p -value 1 without FBS).

2.6. Applications in 3D Synthetic Hydrogels

Several synthetic in vitro platforms have been developed to compete with naturally derived materials like collagen gel and Matrigel, as the synthetic materials enable more tunability and precise control over their properties than protein-based hydrogels.^[23] We cultured HCC1143 in 3D poly(ethylene glycol) (PEG) hydrogels containing the widely used integrin-binding peptide sequence Arg-Gly-Asp (RGD), partially crosslinked with a matrix metalloproteinase (MMP) sensitive peptide. Cells proliferated more in the degradable PEG-RGD hydrogels than in the non-degradable hydrogels (Figure 4d). Less cell death and faster cell growth were achieved in growth media condition supplemented with epithelial growth factor (EGF) than in regular serum containing media, but the dormant cell population did not change significantly (p -value 1) upon EGF addition (Figure 4d and Figure S4d, Supporting Information). This suggests that the addition of growth factors influences cell proliferation, but does not play a significant role in dormant cell populations in 3D synthetic PEG-RGD hydrogels. The presence of MMP-degradable sites in the 3D synthetic environment resulted in fewer nondividing cells, but this trend was not statistically significant (p -value 0.36 in 10% serum, and 0.64 in 10% serum + EGF).

2.7. Cell Clonality Differences in Dormancy Tracking

Thus far, all studies were performed on heterogeneous cell lines, where observations could be determined by both microenvironment and the genetic differences within these populations. Thus, we created cell subclones from the otherwise heterogeneous MDA-MB-231 cells, a triple negative breast cancer cell line,^[33] and its cell subclones were cultured in PEG-RGD hydrogels of 2 kPa modulus with MMP-degradable sites. Although the subclones originated from the same cell line, their proliferation, death, and dormancy rates varied, demonstrating the power of cell intrinsic factors in driving dormancy and growth (Figure 4e,f and Figure S4e, Supporting Information). However, the differences across the cell subclones were not statistically significant. This implies that differences observed across the unique cell lines we tested were much stronger than when comparing across available cell subclones within a single cell line. Together, these results conclude that the cell lineage tree analysis can be used to analyze growth behavior of cells of various subtypes on diverse culturing environments to track and identify individual dormant cells while keeping them alive.

2.8. Serum Recovery Triggers Dormant Cells to Resume Proliferation

Truly dormant cells should be able to restimulate proliferation under appropriate environmental contexts. Thus far, our data

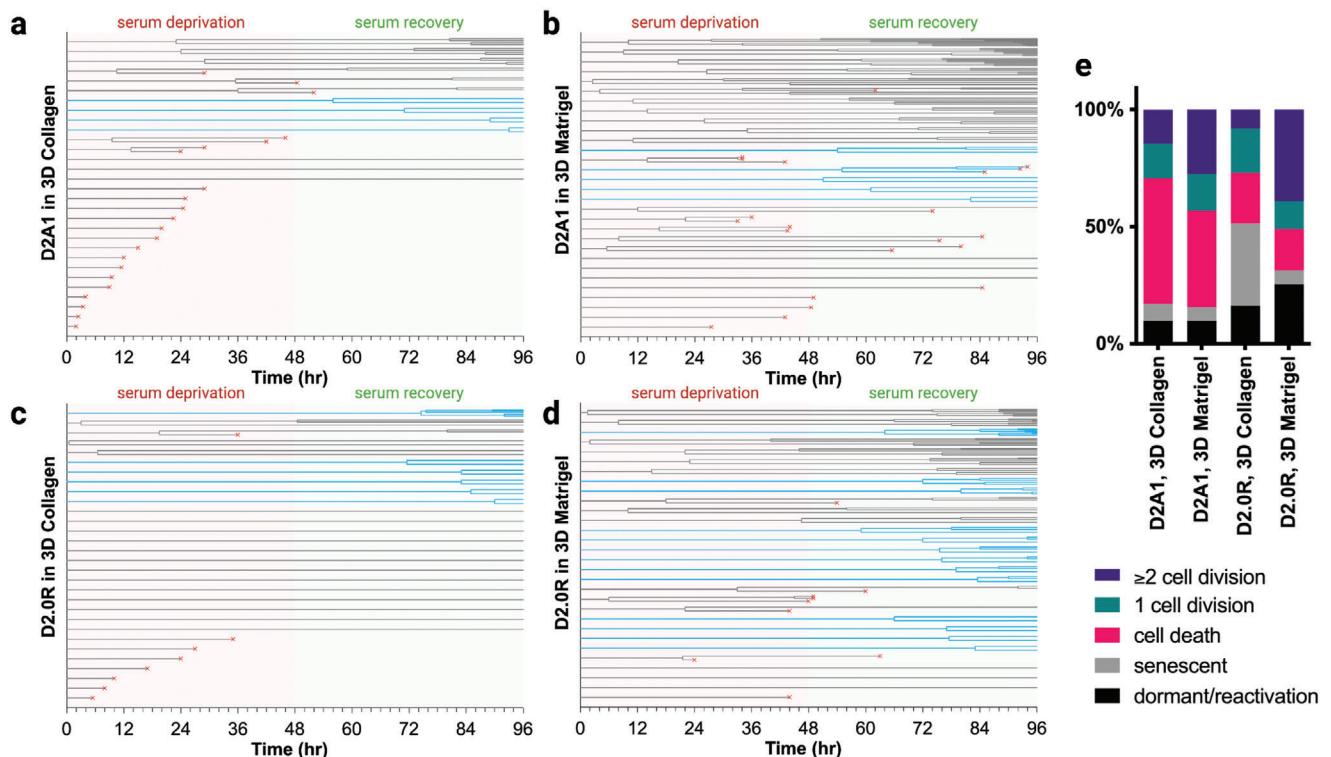


Figure 5. Cell lineage tracing of D2 series cells in 3D collagen and Matrigel during serum recovery. Cell lineage analysis for a) D2A1 in 3D collagen, b) D2A1 in 3D Matrigel, c) D2.0R in 3D collagen, and d) D2.0R in 3D Matrigel. Imaging started from Time = 0 h in the graphs, 6 h after serum deprivation started. 48 h after imaging cells under serum deprivation, we placed full serum media (10% FBS) and continued imaging for additional 48 h. Blue horizontal lines indicate the cells that showed proliferation during the 48-h serum recovery window. e) Stacked bar graphs showing the distribution of each cell population, such as dormant/reactivation, senescent, cell death, one cell division, and two or more cell divisions during 96-h tracing.

have shown only lacked proliferation over 50 h of imaging, and these cells could be either dormant or senescent (permanently exiting the cell cycle). To distinguish between dormant and senescent cells, we reintroduced serum (10% FBS) to D2A1 and D2.0R cells cultured in 3D collagen and Matrigel after a serum deprivation period, and continued imaging for an additional 48 h (Figure 5). A greater fraction of D2.0R cells resumed proliferation during serum recovery, compared to the D2A1 line when comparing across the same environment (p -value 0.3692 in collagen, 0.3618 in Matrigel). More strikingly, the dormant cell population varied significantly in D2.0R cell lines under different environmental conditions (collagen vs Matrigel, p -value 0.0060). These data show that serum recovery triggers quiescent cells to re proliferate, allowing us to distinguish dormant cells (Video S3, Supporting Information) from possibly senescent cells (Video S4, Supporting Information).

3. Discussion

Here, we adapted a live cell tracking approach, where we can, in real time, with living cells, distinguish quickly between actively dividing cells, dying cells, and quiescent cells without the need for a fluorescent reporter. When combined with immunofluorescent staining at the end of the experiment, we can confirm which quiescent cells were in a dormant state using an accepted set of dormancy markers (Ki67-low, ERK-low, and p38-high).^[34,35]

Combined with statistical analyses, information about these individual cells can go even further, revealing a rich data set where we can extract differences in both intrinsic and extrinsic regulators of proliferation versus quiescence. By combining lineage tracing with control over tumor cell environments, we propose this as a method to carefully examine cellular dormancy over a near limitless extracellular parameter space.

To demonstrate the feasibility of this approach, we tracked individual cells from several different breast cancer cell lines (ER⁺ MCF7, HER2⁺ HCC1954, TNBC MDA-MB-231, subclones of those MDA-MB-231s, TNBC HCC1143, and the murine TNBC D2.A1 and D2.0R lines) across several different microenvironments (on TCPS, protein- and peptide-coupled glass surfaces, thin layers of collagen and Matrigel, in 3D collagen and Matrigel, and in synthetic PEG-RGD gels). Our motivation for analyzing this broad set of cell lines is that they span the commonly used extrinsic subtypes of breast cancer. These subtypes are associated with specific rates and regions of recurrence.^[36,37] TNBC has the highest rate of recurrence in the first five years, whereas the recurrence rate for luminal A and luminal B tumors is initially low, but remains continuous even after 10 years of follow-up.^[36] Among several breast cancer subtypes, estrogen receptor positive (ER⁺) breast cancer is most commonly associated with bone metastasis and dormancy.^[32] Although using only a small set of cell lines does not necessarily reflect the heterogeneity in these subtypes, applying the lineage tracing allowed us to observe

microenvironmental (ECM and serum) regulation of dormant states across representatives of these subtypes.

The largest drivers of variability in dormancy versus growth in our studies were cell line source, serum, and collagen. The most obvious example is when we compared the proliferative D2A1 cells to the dormant D2.0R cells, which have obvious phenotypic differences even though derived from the same tumor source. In serum, both these cells are highly proliferative, but when under serum-deprivation stress, the D2A1 cells have a bimodal population containing either proliferative or dying cells but minimal dormant cells. In contrast, the D2.0R cells shift to a population containing many dormant cells (Figure 3). Dormancy dependence on serum was also highly cell line dependent; while the D2 series cells were highly serum dependent, we saw minimal population shifts when we toggled serum for the HCC1954 cells across microenvironments (Figure 2), the MCF7 cells (Figure 2), or the MDA-MB-231 parental or cell line subclones (Figure 4). This general concept—that intrinsic cell line differences determine dormancy capacity—aligns with a previous study by Kloxin group, who showed that cell line subtypes showed distinct dormancy scores when they controlled for the microenvironment in a long-term 3D dormancy culture model.^[16] In their synthetic matrix, ER+ breast cancer cells underwent dormancy while triple negative breast cancer cells did not.^[16]

For one cell line (HCC1954), we applied our cell lineage tracing approach across several microenvironments (2D, 3D, collagen, Matrigel, and on collagen-derived peptides). Similar to what we observed in prior work, the highest number of dormant cells were observed on and in collagen-rich environments.^[22] The identity and dimensionality of ECM control of cell growth is well-appreciated.^[38] Specifically for dormant cell behaviors, there are multiple studies that have shown the degradability of materials or immobilization by environment could induce cellular dormancy.^[39,40] For example, hydrogels with no adhesivity but high degradability induced cellular dormancy, while hydrogels with high adhesivity and degradability promoted growth.^[39] Also, nondegradable hydrogels immobilize cells in the microenvironment, and this physical confinement can also promote dormancy.^[40]

One notable limitation of our approach is that it can only quantify cellular dormancy across a population of heterogeneous cells, and not tumor dormancy. Cellular dormancy is when individual cells are quiescent and nonproliferative, and tumor dormancy is when there is an equilibrium between cell proliferation and death across the bulk of the tumor mass.^[41] By individually tracking cells with bright-field microscopy in and on transparent ECMs, we can easily and reliably monitor individual cells, but cannot track individual cells once they grow enough to form small spheroids (Video S5, Supporting Information). Also, when such spheroids grow fast enough to meet single quiescent cells nearby, such quiescent cells will no longer able to track because they merge into or overlap with the spheroids. In such cases, we cannot distinguish dormant cells from senescent cells. In our study, we monitored cellular dormancy by seeding cells at a low enough density to accurately find and track single cells, while avoiding cell clumping. Although our work here followed cells for only days, this could be extended, such as over the course of weeks. This could further improve the accuracy of distinguishing dormant versus slowly proliferating cells. Since this method uses

live microscopy, it could also be combined with live cell reporters of p38 and ERK.

We suggest this cell lineage tracing approach as a simple way to track single cell dormancy,^[18] and we applied it here across a variety of cell line sources and ECM environments. One of the advantages of this method is that we can trace live cells real time unlike other endpoint assays. This will help us to better understand cellular dormancy and how it is related to the tumor microenvironment of DTCs. We propose this approach has a vast array of applications, not limited to dormancy, where knowing the dynamics of a cell population with simple brightfield tracking would be beneficial. For instance, Gross et al. used the cell lineage tree model to capture cell cycle dynamics upon drug application, which includes drug-specific effects on cell cycle phases.^[42] Combined with biomaterials expertise, this approach is powerful to explore which microenvironmental factors are critical for inducing dormancy and reawakening cells. Given the short time frame of these experiments, this is an excellent space in which to quickly hypothesis test regulators of dormancy and reawakening that are much faster than *in vivo* experiments. Future extensions of this work could include selecting individual cells identified via microscopy for additional profiling to understand the molecular basis of ECM-driven dormancy, e.g., spatial transcriptomics.

4. Experimental Section

Breast Cancer Cell Culture: Different types of human breast cancer cell lines, including MCF7, MDA-MB-231, HCC1954, and HCC1143, were used for this study. MCF7 and MDA-MB-231 cells were cultured under 5% CO₂ and 37°C with DMEM containing 10% fetal bovine serum (FBS) and 1% penicillin/streptomycin (pen/strep). MDA-MB-231 cell subclones were generated by Ning-Hsuan Tseng,^[33] and the same culturing method was used as the parental MDA-MB-231 cell line. HCC1954 and HCC1143 were cultured under 5% CO₂ and 37°C with RPMI containing 10% FBS and 1% pen/strep. Two different types of mouse mammary tumor cells were also used, which were derived from spontaneous mouse mammary tumors, originated from D2 hyperplastic alveolar nodule in Miller lab.^[43,44] D2A1 (proliferative) and D2.0R (dormant) cells were cultured under 5% CO₂ and 37°C with DMEM containing 10% FBS and 1% pen/strep.

Live Cell Microscopy for Tracing Individual Cells: Cells were seeded on TCPS, functionalized glass coverslips, 2D collagen gel, 2D Matrigel, or in 3D collagen gel or 3D Matrigel. The cell culture media was changed 24 h after cell seeding, to either normal growth medium (with 10% FBS) or serum-free medium. Six hours after the media change, time-lapse images of single cells were taken for 50 h, at either 15-min (for 2D experiments) or 30-min intervals (for 3D experiments). Imaging was performed using Zeiss Axio Observer Z1 Inverted Fluorescence Microscope.

Preparation of Culturing Environment and Cell Seeding for 2D Environment: For TCPS: After reaching at least 80% confluence in T-25 flasks, cells were harvested and seeded on different substrates with varying media conditions. Roughly 2 mL of 1x PBS was used to wash the flask before using 2 mL trypsin for 2–5 min to cleave cells off flask surface. The trypsin was then deactivated with 4 mL of regular media. The gathered liquid and cells were placed in a 10 mL conical tube and centrifuged for 5 min at 200×g. The cell pellet was aspirated by vacuuming the supernatant and the cells were resuspended in 1 mL of media. The cells were counted using an automated cell counter (a hemocytometer was used with near similar results). After seeding cells at 1000 cells per well in a 24-well plate, cells were incubated for 24 h to adhere before changing media conditions (serum-free DMEM and RPMI media). An additional 6 h incubation occurred before beginning imaging for 50 h.

For 2D Matrigel: Matrigel (Corning) was thawed overnight in the 4°C fridge to prepare for use the following day. 80% confluence was achieved

in T-25 flasks, and then the cells were harvested to use with different growing medium on top of the Matrigel. Once completely sterilized, 100 μ L Matrigel was slowly pipetted into a warm 96-well plate, and then was placed to polymerize in the 37°C incubator for 20 min. While waiting for the Matrigel to solidify, the same cell harvesting procedure as described for the TCPS method was used. A 200-cell density in each well placed in 100 μ L of media to seed on top of the Matrigel layer was calculated. We waited 24 h for cells to adhere before changing media conditions and imaging (Figure 1c).

For 2D collagen gel: Rat tail collagen I was taken out of 4°C fridge and kept on ice. 410 μ L of rat tail collagen I solution at 3 mg mL⁻¹ was mixed with 520 μ L of serum-free media and 25 μ L of sterile-filtered 1 M NaOH in microcentrifuge tubes, final concentration of which is 1.3 mg mL⁻¹. 100 μ L of this mixture solution was taken and placed into a prewarmed 96-well plate, which was then placed to polymerize in the 37°C insulator for 30 min. While waiting for the collagen gels to polymerize, the same cell harvesting procedure as described in the TCPS method was used. 200 cells per well were seeded on top of each 2D collagen gel in a 96-well plate, and 100 μ L of media was placed on top. After 24 h, the media was exchanged with or without serum and imaging (Video S6, Supporting Information).

For 2D-functionalized coverslips: Rat tail collagen I protein and collagen I integrin-binding peptide were immobilized on glass coverslips. Briefly, 15 mm coverslips were oxygen plasma treated (Harrick Plasma, Ithaca, NY), and silanized through vapor phase deposition of (3-aminopropyl)triethoxysilane (Sigma-Aldrich) at 90°C for a minimum of 18 h. The coverslips were sequentially rinsed in toluene (Fischer Scientific), 95% ethanol (Decon Laboratories, King of Prussia, PA, USA), and water, and dried at 90°C for 1 h. These were subsequently functionalized with 10 g L⁻¹ N,N-disuccinimidyl carbonate (Sigma-Aldrich) and 5% v/v diisopropylethylamine (Sigma-Aldrich) in acetone (Fischer Scientific) for 2 h. Finally, coverslips were rinsed three times in acetone and air-dried for 10 min. Rat tail collagen I protein and collagen I integrin-binding peptide were then covalently bound to the glass coverslips via the reactive amines at 2 μ g cm⁻² concentration. The peptide sequence CGPGPPGPPGPPGPPGPPGFOGERGPPGPPGPPGPP (GFOGER) was used as the collagen I binding peptide. The rat tail collagen I protein and GFOGER peptide were subsequently blocked using methyl-PEG24-amine (MA-PEG24) (Thermo Fisher Scientific). Post functionalization, the coverslips were UV-sterilized for minimum of 1 h. The cells were then added on the coverslips. In prior trials, it was noted that the cells adhered less to coverslips, thus a higher amount of cells (4000 cells per well in a 24-well plate) were seeded compared to 1000 cells on plastic, so that the cell numbers during analysis were comparable between the two substrates. The cells were allowed to adhere on the surface before changing the media and imaging (Figure 1d).

Preparation of Culturing Environment and Cell Seeding for 3D Environment: For 3D Matrigel: Matrigel was thawed overnight in the 4°C fridge and the Matrigel was placed on ice on the day of experiment. For all the cell lines except for D2 series and MDA-MB-231 cells, 5000 cells were mixed with 10 μ L of Matrigel, the 10 μ L of Matrigel was placed on a prewarmed 24-well plate, and the plate was put in the 37°C incubator for 20 min to fully polymerize Matrigel. Once polymerized, 1 mL of media was put in each well. D2 series and MDA-MB-231 cells were seeded at 1000 cells per 10 μ L gel; the faster growth rate than others meant that fewer cells were needed to be placed to make cells sparse enough for analysis.

For 3D collagen gel: Rat tail collagen I was taken out of the 4°C fridge and kept on ice. 41 μ L of rat tail collagen I solution at 3 mg mL⁻¹ was mixed with 52 μ L of serum-free media and 2.5 μ L of sterile filtered 1 M NaOH in microcentrifuge tubes, final concentration of which is 1.3 mg mL⁻¹. 90 μ L of this mixture solution was taken out to resuspend cell pellets of 45000 cells in nine collagen gels. 10 μ L of this solution was used to make one collagen gel with 5000 cells per gel in a 24-well plate for all cell lines except for D2 series cells and MDA-MB-231 cells. Once polymerized, 1 mL of media was placed in each well. D2 series and MDA-MB-231 cells were seeded at 1000 cells per 10 μ L gel. They grow faster than the others, and so fewer cells were placed to make cells sparse enough for analysis.

For 3D PEG-RGD gel: 20 kDa four-arm PEG-maleimide (JenKem Technology) was dissolved in serum-free media at pH 7.4 and 20 wt%, mixed with 2×10^{-3} M RGD peptide (peptide sequence: GRGDSPCC) purchased

from GenScript, and let react at room temperature for 10 min. RGD peptides were used as integrin-binding peptides. 1.5 kDa PEG-dithiol (JenKem Technology) was dissolved in 1x PBS at pH 7.4. The weight of PEG-dithiol was calculated to have 1:1 molar ratio of thiol to maleimide when mixed together. The PEG-dithiol solution was mixed with 25 mol% of MMP-degradable peptide, GCRDGPQGIWGQDRCG, purchased from GenScript for the PEG-RGD gels with degradable sites. 1 μ L of PEG-dithiol solution was placed first in the middle of the well on a 24-well plate, followed by an addition of 9 μ L of PEG-maleimide solution with peptides and cells on top of the 1 μ L PEG-dithiol solution. 10000 cells per gel were seeded in each 10 μ L gel, and 1 mL of media was placed in the 24-well plate after letting the gels to fully polymerize for 5–10 min in the 37°C incubator. 24 h after gelation, the culture media was changed to serum-containing or serum-free media, followed by 50-h imaging for cell lineage tree analysis (Video S7, Supporting Information).

Lineage Tree Analysis: After the 50-h imaging was done on a Zeiss Axio Observer Z1 Inverted Fluorescence Microscope, all the microscope image files were transferred to open in Imaris software. Microscope files were then converted to movie files showing a timeline as seen in the videos of each cell population (dividing, dying, quiescent) (Videos S1–S4, Supporting Information). Specific time points when a cell divides or dies were manually marked on an Excel spreadsheet for randomly selected cells in each condition, which generated cell lineage trees to illustrate individual cell growth.

As seen in Figure 1a, each horizontal line indicates a single cell during the multihour time-lapse microscopy imaging. When a cell divides, the horizontal line diverges at that time point. When a cell dies, it is marked with a red “x” at the end. Single horizontal lines that do not diverge throughout the whole time of imaging indicate cells that did not divide but are still alive for the entire period of time-lapse microscopy imaging.

From each cell lineage tree, the numbers of nondividing and dying cells, as well as the number of cells that divide once or that divide two or more times, were counted during the 50-h imaging. Stacked bar graphs were created in Prism software, visualizing the proportion of cells in each category (no division; cell death; 1 cell division; ≥ 2 cell division) (Figure 1c).

Immunofluorescence Staining and Imaging: After the 50-h imaging was finished, cells were fixed with 10% formalin. Cells were then permeabilized and stained with DAPI, Ki-67 (ab156956, Abcam), ERK (ab54230, Abcam), and p38 (#4511, CellSignaling). IF-stained cells were imaged using Zeiss Cell Observer SD Spinning Disc Confocal Microscope.

Statistical Analysis: Two-sided Fisher exact test was performed to determine whether the association between the categories (e.g., dormant versus nondormant cells) is significant under various conditions. The open source Scipy library from Python 3.9 and Prism software were used to calculate the *p*-value.

Supporting Information

Supporting Information is available from the Wiley Online Library or from the author.

Acknowledgements

The authors would like to thank Sean Gross for help with learning the cell lineage tracing approach. The authors would also like to thank Ning-Hsuan Tseng for providing the cell subclones of MDA-MB-231 cell line. This work was supported by a grant from the Jayne Koskinas Ted Giovanis Foundation for Health and Policy, an NSF CAREER grant (DMR-1454806), and grants from the NIH (R21-CA223783, DP2-CA186573, and U01-CA265709) to S.R.P. S.R.P. was supported by an Armstrong Professorship at UMass Amherst. This work was also supported by a grant from the NIH (U01-CA215709) to A.S.M., and a grant from the NIH (U54-CA209988) to L.M.H.

Conflict of Interest

The authors declare no conflict of interest.

Data Availability Statement

The data that support the findings of this study are available from the corresponding author upon reasonable request.

Keywords

biomaterials, breast cancer, collagen, Matrigel, poly(ethylene glycol) hydrogels

Received: September 5, 2022

Revised: December 2, 2022

Published online: January 20, 2023

- [1] L. A. Torre, F. Islami, R. L. Siegel, E. M. Ward, A. Jemal, *Cancer Epidemiol. Biomarkers Prev.* **2017**, *26*, 444.
- [2] H. Sung, J. Ferlay, R. L. Siegel, M. Laversanne, I. Soerjomataram, A. Jemal, F. Bray, *CA-Cancer J. Clin.* **2021**, *71*, 209.
- [3] C. Allemani, H. K. Weir, H. Carreira, R. Harewood, D. Spika, X.-S. Wang, F. Bannon, J. v Ahn, C. J. Johnson, A. Bonaventure, R. Marcos-Gragera, C. Stiller, G. Azevedo e Silva, W.-Q. Chen, O. J. Ogundiyi, B. Rachet, M. J. Soeberg, H. You, T. Matsuda, M. Bielska-Lasota, H. Storm, T. C. Tucker, *Lancet* **2015**, *385*, 977.
- [4] C. Allemani, T. Matsuda, V. di Carlo, R. Harewood, M. Matz, M. Nikšić, A. Bonaventure, M. Valkov, C. J. Johnson, J. Estève, O. J. Ogundiyi, G. A. E. Silva, W.-Q. Chen, S. Eser, G. Engholm, C. A. Stiller, A. Monnereau, R. R. Woods, O. Visser, G. H. Lim, J. Aitken, H. K. Weir, M. P. Coleman, *Lancet* **2018**, *391*, 1023.
- [5] C. A. Anyigba, G. A. Awandare, L. Paemka, *Exp. Biol. Med.* **2021**, *246*, 1377.
- [6] A. Weiss, M. Chavez-MacGregor, D. Y. Lichtensztajn, M. Yi, A. Tadros, G. N. Hortobagyi, S. H. Giordano, K. K. Hunt, E. A. Mittendorf, *JAMA Oncol.* **2018**, *4*, 203.
- [7] N. Howlader, A. M. Noone, M. Krapcho, D. Miller, K. Bishop, S. F. Altekruse, C. L. Kosary, M. Yu, J. Ruhl, Z. Tatalovich, A. Mariotto, D. R. Lewis, H. S. Chen, E. J. Feuer, K. A. Cronin, *Cancer Statistics Review*, National Cancer Institute, Bethesda, MD **2021**.
- [8] T. N. Seyfried, L. C. Huysentruyt, *Crit. Rev. Oncog.* **2013**, *18*, 43.
- [9] D. M. Sosnoski, R. J. Norgard, C. D. Grove, S. J. Foster, A. M. Mastro, *Clin. Exp. Metastasis* **2015**, *32*, 335.
- [10] A. B. Shupp, A. D. Kolb, D. Mukhopadhyay, K. M. Bussard, *Cancers* **2018**, *10*, 182.
- [11] P. Carlson, A. Dasgupta, C. A. Grzelak, J. Kim, A. Barrett, I. M. Coleman, R. E. Shor, E. T. Goddard, J. Dai, E. M. Schweitzer, A. R. Lim, S. B. Crist, D. A. Cheresh, P. S. Nelson, K. C. Hansen, C. M. Ghajar, *Nat. Cell Biol.* **2019**, *21*, 238.
- [12] H. Endo, M. Inoue, *Cancer Sci.* **2019**, *110*, 474.
- [13] C. M. Ghajar, H. Peinado, H. Mori, I. R. Matei, K. J. Evason, H. Brazier, D. Almeida, A. Koller, K. A. Hajjar, D. Y. R. Stainier, E. I. Chen, D. Lyden, M. J. Bissell, *Nat. Cell Biol.* **2013**, *15*, 807.
- [14] S. Malladi, D. G. Macalinao, X. Jin, L. He, H. Basnet, Y. Zou, E. de Stanchina, J. Massague, *Cell* **2016**, *165*, 45.
- [15] A. Micalet, E. Moeendarbary, U. Cheema, *ACS Biomater. Sci. Eng.* **2021**, <https://doi.org/10.1021/acsbiomaterials.0c01530>.
- [16] E. M. Ovadia, L. Pradhan, L. A. Sawicki, J. E. Cowart, R. E. Huber, S. W. Polson, C. Chen, K. L. van Golen, K. E. Ross, C. H. Wu, A. M. Kloxin, *Adv. Biosyst.* **2020**, *4*, 2000119.
- [17] S. Pradhan, J. H. Slater, *Biomaterials* **2019**, *215*, 119177.
- [18] F. Mohammadi, S. Visagan, S. M. Gross, L. Karginov, J. C. Lagarde, L. M. Heiser, A. S. Meyer, *bioRxiv* **2021**, 2021.06.25.449922.
- [19] A. A. Stepanenko, V. V. Dmitrenko, *Gene* **2015**, *574*, 193.
- [20] L. E. Barney, E. C. Dandley, L. E. Jansen, N. G. Reich, A. M. Mercurio, S. R. Peyton, *Integr. Biol.* **2015**, *7*, 198.
- [21] E. A. Brooks, L. E. Jansen, M. F. Gencoglu, A. M. Yurkevicz, S. R. Peyton, *ACS Biomater. Sci. Eng.* **2018**, *4*, 707.
- [22] L. E. Barney, C. L. Hall, A. D. Schwartz, A. N. Parks, C. Sparages, S. Galarza, M. O. Platt, A. M. Mercurio, S. R. Peyton, *Sci. Adv.* **2020**, *6*, eaaz4157.
- [23] G. Rijal, W. Li, *Biomaterials* **2016**, *81*, 135.
- [24] R. Edmondson, A. F. Adcock, L. Yang, *PLoS One* **2016**, *11*, e0158116.
- [25] C. Josan, S. Kakar, S. Raha, *Adipocyte* **2021**, *10*, 361.
- [26] G. N. Naumov, I. C. MacDonald, P. M. Weinmeister, N. Kerkvliet, K. V. Nadkarni, S. M. Wilson, V. L. Morris, A. C. Groom, A. F. Chambers, *Cancer Res.* **2002**, *62*, 2162.
- [27] G. N. Naumov, J. L. Townson, I. C. MacDonald, S. M. Wilson, V. H. C. Bramwell, A. C. Groom, A. F. Chambers, *Breast Cancer Res. Treat.* **2003**, *82*, 199.
- [28] V. L. Morris, A. B. Tuck, S. M. Wilson, D. Percy, A. F. Chambers, *Clin. Exp. Metastasis* **1993**, *11*, 103.
- [29] V. L. Morris, S. Koop, I. C. MacDonald, E. E. Schmidt, M. Grattan, D. Percy, A. F. Chambers, A. C. Groom, *Clin. Exp. Metastasis* **1994**, *12*, 357.
- [30] J. Fares, M. Y. Fares, H. H. Khachfe, H. A. Salhab, Y. Fares, *Signal Transduction Targeted Ther.* **2020**, *5*, 28.
- [31] R. R. Gomis, S. Gawrzak, *Mol. Oncol.* **2017**, *11*, 62.
- [32] R. E. Coleman, R. D. Rubens, *Br. J. Cancer* **1987**, *55*, 61.
- [33] N.-H. Tseng, *Extracellular Matrix Stiffness as a Cue to Shape Phenotypic Evolution of Triple Negative Breast Cancer*, University of Massachusetts, Amherst, MA **2022**.
- [34] L. J. Gay, I. Malanchi, *Biochim. Biophys. Acta, Rev. Cancer* **2017**, *1868*, 231.
- [35] M. S. Sosa, P. Bragado, J. A. Aguirre-Ghiso, *Nat. Rev. Cancer* **2014**, *14*, 611.
- [36] A. Ignatov, H. Eggemann, E. Burger, T. Ignatov, *J. Cancer Res. Clin. Oncol.* **2018**, *144*, 1347.
- [37] R. Yerushalmi, R. Woods, H. Kennecke, C. Speers, M. Knowling, K. Gelmon, *Breast Cancer Res. Treat.* **2010**, *120*, 753.
- [38] K. F. Ruud, W. C. Hiscox, I. Yu, R. K. Chen, W. Li, *Breast Cancer Res.* **2020**, *22*, 82.
- [39] C. J. F. Reyes, S. Pradhan, J. H. Slater, *Adv. Healthcare Mater.* **2021**, *10*, 2002227.
- [40] J. A. Preciado, E. Reátegui, S. M. Azarin, E. Lou, A. Aksan, *Technology* **2017**, *5*, 129.
- [41] J. Dittmer, *Semin. Cancer Biol.* **2017**, *44*, 72.
- [42] S. M. Gross, F. Mohammadi, C. Sanchez-Aguila, P. J. Zhan, A. S. Meyer, L. M. Heiser, *bioRxiv* **2021**, 2020.07.24.219907.
- [43] F. R. Miller, D. McEachern, B. E. Miller, *Cancer Res.* **1989**, *49*, 6091.
- [44] J. W. Rak, D. McEachern, F. R. Miller, *Br. J. Cancer* **1992**, *65*, 641.